

Effect of polarity on beam and plasma target formation in a dense plasma focus

Cite as: Phys. Plasmas **26**, 042702 (2019); <https://doi.org/10.1063/1.5048423>

Submitted: 13 July 2018 . Accepted: 17 March 2019 . Published Online: 10 April 2019

S. Jiang , D. P. Higginson , A. Link, I. Holod, and A. Schmidt



View Online



Export Citation



CrossMark

ARTICLES YOU MAY BE INTERESTED IN

[Ignition threshold in cylindrical fast ignition targets](#)

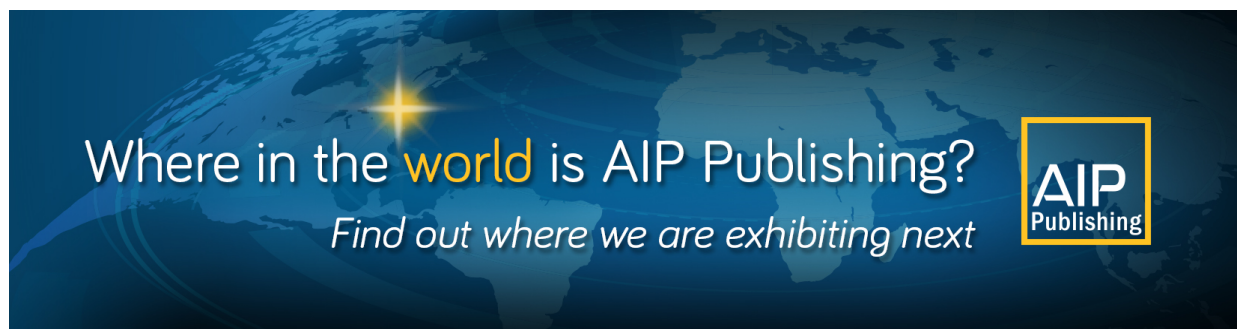
Phys. Plasmas **26**, 042703 (2019); <https://doi.org/10.1063/1.5050964>

[Acceleration of charged particles to extremely large energies by a sub-Dreicer electric field](#)

Phys. Plasmas **26**, 042102 (2019); <https://doi.org/10.1063/1.5081716>

[Measurement of wave-particle interaction and metastable lifetime using laser-induced fluorescence](#)

Phys. Plasmas **26**, 042111 (2019); <https://doi.org/10.1063/1.5089178>



Effect of polarity on beam and plasma target formation in a dense plasma focus

Cite as: Phys. Plasmas **26**, 042702 (2019); doi: [10.1063/1.5048423](https://doi.org/10.1063/1.5048423)

Submitted: 13 July 2018 · Accepted: 17 March 2019 ·

Published Online: 10 April 2019



View Online



Export Citation



CrossMark

S. Jiang,^{a)} D. P. Higginson, A. Link, I. Holod, and A. Schmidt

AFFILIATIONS

Lawrence Livermore National Laboratory, 7000 East Ave, Livermore, California 94550, USA

Note: This paper is part of the Special Collection: Papers from the 60th Annual Meeting of the APS Division of Plasma Physics

Note: Paper Q13 3, Bull. Am. Phys. Soc. **63** (2018).

^{a)}Invited speaker.

ABSTRACT

Dense plasma focus (DPF) devices are conventionally operated with a polarity such that the inner electrode (IE) is the anode. It has been found that interchanging the polarity of the electrodes (i.e., IE as the cathode) can cause an order of magnitude decrease in the neutron yield. This polarity riddle has previously been studied empirically through several experiments and is yet not well understood. We have performed kinetic simulations using the particle-in-cell modeling to investigate the problem. This is the first time that both polarities have been studied with simulations in great detail. In our simulations, we have modeled the entire beam and plasma target formation processes, but we did not consider differences in break-down conditions caused by the two polarities. We have found that when using reverse polarity ions are still accelerated and, in fact, attain similar energy spectra as in the standard polarity case. The difference is that the fields are flipped and thus ions are accelerated in the opposite direction. So, in the reverse polarity case, the majority of the “plasma target” (formed by the imploding plasma) is in the opposite direction of the beam, and thus, the beam hits the IE and produces few neutrons. With a better inner electrode configuration, reverse polarity is able to create a high-quality ion beam as well as a high-density target. Both can be comparable to that generated by standard polarity. Furthermore, we will show that it is easier to add an additional solid catcher target to a DPF device with reverse polarity, potentially enabling it to generate more neutrons than standard polarity.

Published under license by AIP Publishing. <https://doi.org/10.1063/1.5048423>

I. INTRODUCTION

A dense plasma focus (DPF) can serve as a portable device for intense electron, ion, X-ray, and neutron sources.^{1–4} A DPF is composed of two coaxial cylindrical electrodes with a low-pressure gas fill between them. A schematic plot of a typical DPF is shown in Fig. 1, with the yellow, gray, and white blocks indicating the inner electrode (IE), outer electrode (OE), and insulator, respectively. When a high-pulsed voltage is applied, the gas at the surface of the insulator first breaks down and forms a plasma sheath, within which a large current from the anode to cathode flows. The $\mathbf{J} \times \mathbf{B}$ force then pushes the sheath down the inner electrode. As the sheath runs down, it ionizes and sweeps the neutral gas as it accelerates. After the leading front of the sheath reaches the end of IE, it begins to run-in radially, until it eventually implodes on axis, where it generates a short-lived, high-density, high-temperature plasma pinch region. At this point, strong electric fields are formed, causing ions and electrons to be accelerated to high energy (>100 keV). If fusion reactants are used (e.g., deuterium), a bright neutron source is created.

DPF devices are normally operated with the inner electrode as the anode and the outer electrode as the cathode. For this paper, we will refer to this setup as “standard” polarity, and the opposite IE: –, OE: + as “reverse” polarity. Previous experiments have shown that interchanging the electrodes from standard to reverse polarity can cause orders of magnitude decrease in the neutron yield.^{5–11} While symmetry holds regardless of the direction that current flows, the bewildering difference in yield was first raised by Decker *et al.*⁵ as the “polarity riddle.” He studied a fast plasma focus device (SPEED 1) with a 20 kJ energy, a 160 kV voltage, and a 400 ns rise time. The results showed that without shielding of the radial electric field from the insulator surface, the neutron yield dropped by two orders of magnitude on interchanging the polarity from standard to reverse. After the radial electric field was shielded, the neutron outputs differed by a factor of approximately 6–7. He concluded that the negative field from reverse polarity could prevent desirable sheath build up by pushing the electrons away from the insulator surface, resulting in poor break-down which caused a poor neutron yield. The problem could be

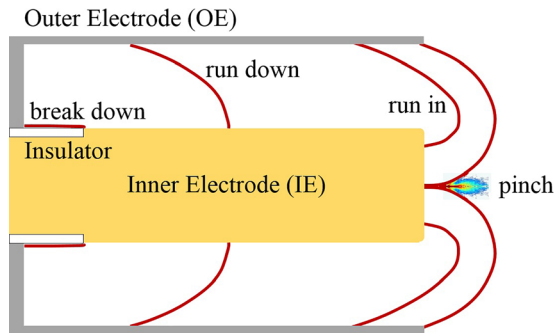


FIG. 1. Schematic plot of a dense plasma focus device and its 4 stages of operation, including break-down, run-down, run-in, and pinch.

substantially mitigated by proper shielding. Decker attributed the decrease in yield to the conditions at break-down and sheath formation. However, even after ruling out the influence of break-down with the shielding, there was still 6–7 times difference in yield between the two polarities, which is the discrepancy that we are trying to address in this paper. Other earlier investigation in polarity riddle involves the optimization of the focus with both polarities. Mathuthu *et al.*^{6,7} built a 2.3 kJ, 12 kV DPF with a negative inner electrode. They did a length scan of the IE and found that the quality of the focus was improved as the electrode length was reduced. For a similar scale DPF with positive polarity, the maximum neutron yield (1.3×10^8) was found at an IE length of 148 mm with a gas pressure of 3.8 Torr.^{12–14} In Mathuthu’s reverse polarity device, the optimized IE length for good focus action is about 40 mm. The authors suggested that one possible reason for the lower neutron yield with reverse polarity could be that more material from IE gets ablated when it is negative; therefore, reducing the IE length from 150 to 40 mm balances this adverse effect.⁷

Apart from the papers mentioned above, we were not able to find any other DPF devices that were operated under reverse polarity. In fact, reverse polarity was not commonly used due to its historical low neutron yield in the above-mentioned experiments. The explanations so far have been very few and mostly empirical. In this paper, we try to solve the polarity riddle using 2D particle-in-cell (PIC) simulations. This is the first time that different phases in plasma focus with both polarities have been studied quantitatively in simulations. In this paper, we will show that apart from the reasons explained in the previous studies, we find that a major effect of reverse polarity on the significant decrease in neutron yield is largely dependent on directionality of the ion beam with respect to the plasma target. We will show that reverse polarity does not necessarily reduce the neutron yield with certain IE designs. In fact, a suitable negative IE has an advantage that it could potentially be coated with a deuterated material and work as a catcher target for D-D fusion, which could increase the yield further.

In past experiments with reverse polarity,^{5–7,11} the inner electrode used was either solid or had only a very small hole in its center. Since the pinch happens close to the tip of the IE, the IE shape can greatly affect the pinch formation. To study this effect, we tried two different IE configurations, one with a solid cylinder to compare with previous experiments and the other with a wide hollow to improve the yield of the reverse polarity case, as shown in Figs. 2(a) and 2(b). For reverse polarity, these two geometries can have completely different outcomes.

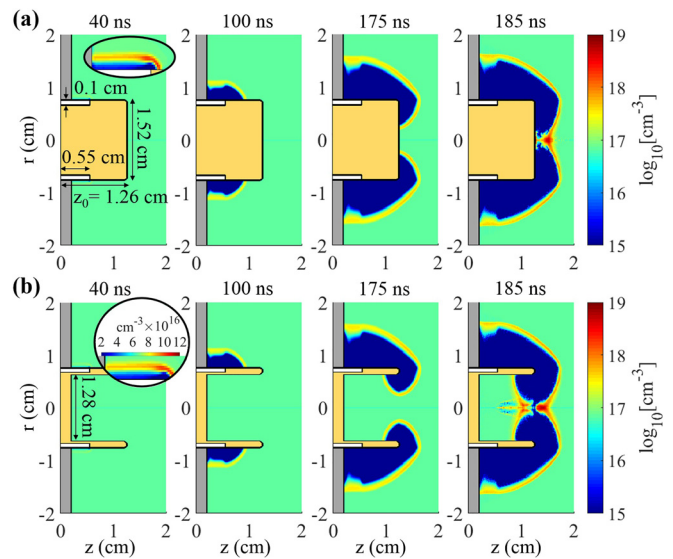


FIG. 2. The deuteron ion density (on a log scale) during 4 different stages of a typical DPF (break-down, run-down, run-in, and pinch from left to right). The insets in the leftmost plots show the D density on a linear scale so that the break-down process is easier to see. The 4 snapshots are taken at 40 ns, 100 ns, 175 ns, and 185 ns from our simulations with standard polarity. (a) and (b) show two different DPF configurations used in the simulations. DPF has standard polarity when the inner electrode is the anode and the outer electrode is the cathode. It has reverse polarity when the inner electrode is the cathode and the outer electrode is the anode.

II. SIMULATION SETUP

We used a similar simulation method as has been reported in previous DPF PIC modeling work.^{15–19} The simulations were carried out using the particle-in-cell code Chicago,²⁰ from the developers of Large Scale Plasma (LSP),²¹ with a direct-implicit scheme.²² They were set up in 2D cylindrical coordinates. The simulation grid is made of 270×400 cells with $\Delta r = \Delta z = 0.01$ cm. The two geometries of the DPF devices are shown in Figs. 2(a) and 2(b). The inner electrode in Fig. 2(a) is a 1.26 cm long solid cylinder with a diameter of 1.52 cm. A second version of the inner electrode, shown in Fig. 2(b), is a tube with the same length and outer diameter but has a hollow inside with a large diameter of 1.28 cm. The rest of the components are the same for (a) and (b). The outer electrode is represented by the gray hollow tube in the plot. The inner electrode is partially covered by a coaxial insulator that is 0.1 cm thick and 0.55 cm long. Note that the thickness of the metal under the insulator in Fig. 2(b) may be too thin to field experimentally, but it does not influence the simulation results since the electrodes were treated as perfect conductors. Both devices are filled with deuterium gas at a pressure of 1 Torr.

An external LRC pulsed power circuit was added at the anode-cathode boundary to include the effects of a finite driver response and energy. The circuit includes 400 nF capacitance, 46 nH inductance, 103 mΩ resistance, and 40 kV voltage, with a total stored energy of 320 Joules. Here, we used a much smaller DPF compared with what Decker *et al.*⁵ used in their paper to reduce the computational cost. As we will show later, we have repeated each run 10 times for good statistics.

Figure 2 shows the 4 stages of discharge evolution in our simulations, including break-down, run-down, run-in, and pinch from left to right, respectively. In the figure, we plot deuteron density on a log scale at 40 ns, 100 ns, 175 ns, and 185 ns. They are all taken from simulations with standard polarity. (a) corresponds to a solid IE and (b) to a hollow IE. The initial stage of the plasma generation is called the break-down. At around 40 ns, a plasma sheet is formed over the insulator surface. It is shown more clearly on a linear scale in the insets. The break-down phase essentially determines the shape of the plasma sheath in the following stages. In our simulations, we did not model the break-down process but instead initialized the plasma with a preformed high-temperature conducting channel at the surface of the insulator. At $t = 0$, the entire volume is filled with a fully ionized room-temperature plasma as ionization is not included in the simulations. In this paper, we do not address the discrepancies in yield at the two polarities associated with differing break-down conditions. The thin plasma sheath then lifts off and is accelerated forward along the axis of the electrode by magnetic field, as is shown in the snapshot at 100 ns. As one would expect, the hollow inside the inner electrode does not affect either the break-down or the run-down, and the sheaths in Figs. 2(a) and 2(b) look identical during the two stages. After the current sheath reaches the end of the inner electrode, the magnetic force causes the sheath to constrict radially. During the run-down and the majority of run-in, the plasma was treated as a quasi-neutral conducting fluid in our simulations.²³ The time step at this stage is 0.01 ns. At 175 ns, the fluid was transitioned to kinetic electrons and ions and then treated in a fully kinetic way later on. The time step was dropped to 2×10^{-3} ns and was adjusted as the magnetic field in the simulation increased, ensuring the resolution of electron cyclotron frequency. Particle collisions were treated using a binary collision algorithm,^{24,25} so that shock heating, viscosity, resistivity, etc., were intrinsically included from a first-principles approach. The shapes of sheath in (a) and (b) are completely different at 175 ns. Geometry of IE plays a significant role during the run-in stage. Finally at about 180 ns, the sheath pinches on axis. The initially well-collimated pinch is then broken up by the $m = 0$ instability, resulting in a large electric field. From the snapshots at 185 ns, we can see how the $m = 0$ instability forms in the pinch region. The field is approximately in the same direction as the current flow, meaning that it points away from IE (anode) with standard polarity and towards IE (cathode) with reverse polarity. The deuteron ions are then accelerated by the field in a non-thermal manner, forming a high energy ion beam. The growth of instabilities has been identified in previous PIC simulations as the major cause of beam formation.^{26,27} The accelerated ions further react with the background plasma and produce D-D neutrons. This neutron generation mechanism is called the beam-target mechanism. When a deuterium gas fill is used, both thermonuclear and beam-target fusion mechanisms can occur in DPF plasmas for neutron production. However, in small devices with low current (< 2 MA) as we study in this paper, beam-target is the dominant fusion mechanism.^{26–30} This indicates that only the deuteron target that is located downstream of the beam has an influence on the yield. Therefore, to better understand the neutron production processes with different polarities, we need to compare the quality of both the ion beam and the background plasma target. In our PIC simulations, neutrons were generated using the D-D fusion cross-sections and the relative velocity between individual macroparticles. The neutron yield using this

simulation method has been benchmarked with experimental results on medium/large scale DPF devices in previous work.^{15–17}

Due to the stochastic nature of instabilities, the neutron yield has a large variation from shot to shot in both experiments and simulations. We have performed 10 simulations for each case we studied with identical initial conditions except for random number seed. Interestingly, the IE geometry affects not only the yield but also the variability of the yield.

Although not shown in Fig. 2, the shape of sheath for reverse polarity looks almost identical to that for standard polarity during the break-down, run-down, and run-in stages. However, the behavior during pinch is quite different, as we are going to discuss in Sec. III

III. RESULTS AND DISCUSSION

A. Neutron yield

Figure 3 illustrates the simulation results for the two DPF configurations in Fig. 2 with both polarities. The curves in the figure correspond to mean results averaged over 10 simulations with identical initial conditions and the shaded areas around them indicate the standard deviation of these runs. Figure 3(a) shows the current, I , as a function of time. For all four cases, the length of the anode was adjusted so that the pinch happens at around the peak current to ensure maximum neutron yield. Note that the current trace has an unrealistic drop without showing a rebound. This is because the simulations have some numerical cooling effects as the pinch happens. This effect can potentially decrease predicted neutron yields by providing less current through the pinch but it may also increase the neutron yields by confining the pinch within a smaller volume. Therefore, the

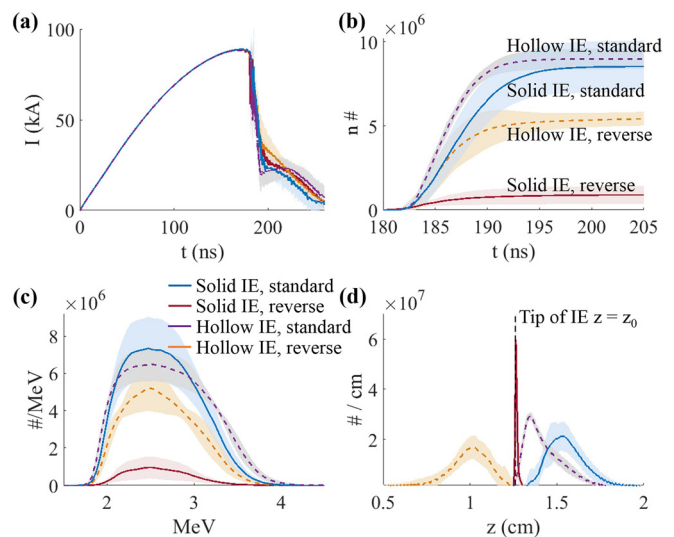


FIG. 3. Simulation results for all 4 different cases, including solid IE with standard polarity (blue), solid IE with reverse polarity (red), hollow IE with standard polarity (purple, dashed), and hollow IE with reverse polarity (orange, dashed). (a) Current as a function of time. (b) Cumulated neutron number as a function of time. (c) Neutron energy spectrum. (d) Neutron birth location dn/dz as a function of z . The results are calculated based on 10 identical runs for either geometry and either polarity. The curves represent the average of the runs and the shaded areas are the standard deviations.

TABLE I. The neutron yield and integrated deuteron cross section for different regions shown in Figs. 5(a1) and 5(b1). The results are calculated based on 10 identical runs for each geometry and each polarity. In this table, the majority region is the region where most of the D ions enter, and the opposite region is the minority region. This means that for standard polarity, Region R is the majority region and Region L is the minority region, while for reverse polarity, Region L is the majority region and Region R is the minority region. The first 3 rows are the neutron yield Y_n . In the next 2 rows, $\int f_D \cdot \sigma dE$ means the integration of deuteron energy spectrum $f_D(E)$ times the thin target D-D cross section. Next, $\int f_D \cdot P_{Inf.D_2} dE$ is the integration of $f_D(E)$ times the neutron generation probability with an infinitely thick D target. This is the maximum neutron yield one can achieve with the given $f_D(E)$. Finally, $\int f_D \cdot P_{Inf.CD_2} dE$ is the integration of $f_D(E)$ times the neutron generation probability with infinite CD_2 . This is the neutron yield from an ideal case when an infinitely thick CD_2 target can be inserted into the device.

IE	Solid IE		Hollow IE	
	Standard +	Reverse -	Standard +	Reverse -
Y_n total ^a	$8.60 \times 10^6 (\pm 18.6\%)$	$8.99 \times 10^5 (\pm 60.9\%)$	$9.14 \times 10^6 (\pm 6.7\%)$	$5.61 \times 10^6 (\pm 8.4\%)$
Y_n majority region ^b	$6.40 \times 10^6 (\pm 18.8\%)$	0	$6.92 \times 10^6 (\pm 6.9\%)$	$5.50 \times 10^6 (\pm 8.4\%)$
Y_n minority region ^c	0	$8.25 \times 10^5 (\pm 61.6\%)$	$7.90 \times 10^4 (\pm 48.7\%)$	$7.08 \times 10^4 (\pm 95.2\%)$
$\int f_D \cdot \sigma dE$, maj. dir. (cm ²)	$1.96 \times 10^{-11} (\pm 18.0\%)$	$3.17 \times 10^{-11} (\pm 15.8\%)$	$1.63 \times 10^{-11} (\pm 6.9\%)$	$1.93 \times 10^{-11} (\pm 12.9\%)$
$\int f_D \cdot \sigma dE$, min. dir. (cm ²)	$3.56 \times 10^{-13} (\pm 118.9\%)$	$1.53 \times 10^{-12} (\pm 224.0\%)$	$3.95 \times 10^{-14} (\pm 74.6\%)$	$2.19 \times 10^{-13} (\pm 91.6\%)$
$\int f_D \cdot P_{Inf.D_2} dE$, maj. dir.	$6.98 \times 10^8 (\pm 15.4\%)$	$9.72 \times 10^8 (\pm 19.9\%)$	$8.85 \times 10^8 (\pm 10.4\%)$	$6.25 \times 10^8 (\pm 24.5\%)$
$\int f_D \cdot P_{Inf.D_2} dE$, min. dir.	$6.19 \times 10^6 (\pm 121.7\%)$	$1.22 \times 10^8 (\pm 275.4\%)$	$1.27 \times 10^5 (\pm 115.4\%)$	$7.04 \times 10^6 (\pm 163.3\%)$
$\int f_D \cdot P_{Inf.CD_2} dE$, maj. dir.	$2.98 \times 10^8 (\pm 14.8\%)$	$4.19 \times 10^8 (\pm 18.3\%)$	$3.68 \times 10^8 (\pm 9.4\%)$	$2.69 \times 10^8 (\pm 22.8\%)$
$\int f_D \cdot P_{Inf.CD_2} dE$, min. dir.	$2.72 \times 10^6 (\pm 121.4\%)$	$4.90 \times 10^7 (\pm 273.4\%)$	$6.24 \times 10^4 (\pm 114.4\%)$	$2.96 \times 10^6 (\pm 157.3\%)$

^aNeutron yield averaged over 10 simulation runs.
^bRegion R for standard polarity, region L for reverse polarity.
^cRegion L for standard polarity, region R for reverse polarity.

exact influence on the neutron yield is still unknown. However, we have verified in these simulations that the majority of deuteron beam formation occurs before the current dips to unrealistically low values and thus we have confidence that our simulated yields are minimally affected by numerical cooling. Our simulations generally reproduce experimental yield within a factor of two and have been benchmarked against DPFs with current ranging from 90 kA to 2.5 MA.^{15–18} The cumulated yield as a function of time is shown in Fig. 3(b). The neutrons were generated within a short period of time between 180 ns and 200 ns. The neutron FWHM pulse length is less than 10 ns. Note that in the simulations we have only recorded the neutron birth time. The time of flight broadening effect would make the pulse more like 50 ns long at a distance of 5 m. The pulse length is actually consistent with the measurements from other small scale DPFs.^{31,32} The total neutron yield can be found in Table I. For solid IE, the yield from reverse polarity is roughly an order of magnitude lower than that from standard polarity, which is consistent with the experimental observation.⁵ However, using a hollow IE shown in Fig. 2(b), the yield from reverse polarity is remarkably enhanced, maintaining greater than 60% of the standard case yield. Another notable feature of the simulations is the run-to-run repeatability in yield, a desirable quality for most applications. Using a solid IE, variation in neutron yield is quite large for both polarities. They are calculated to be 18.6% for standard polarity and 60.9% for reverse polarity. With a hollow IE, the variation is only 6.7% for standard polarity and 8.4% for reverse polarity.

The neutron energy spectra from the simulations are shown in Fig. 3(c). The spectra are peaked at 2.45 MeV. They are all quite asymmetric with respect to the peak position, and their high energy tails extend beyond 4 MeV, indicative of a beam-target fusion mechanism.

Figure 4 shows the neutron birth number density (on a log scale) as a function of r and z in the 2D cylindrical coordinate system. Each

neutron particle in the simulation was recorded at the position where it was born. The apparent “straight lines” in the distribution are indicative of the trajectories of some high energy deuterons that produce neutrons along their way as they transport through the background plasma. This is again the characteristic of a beam-target fusion

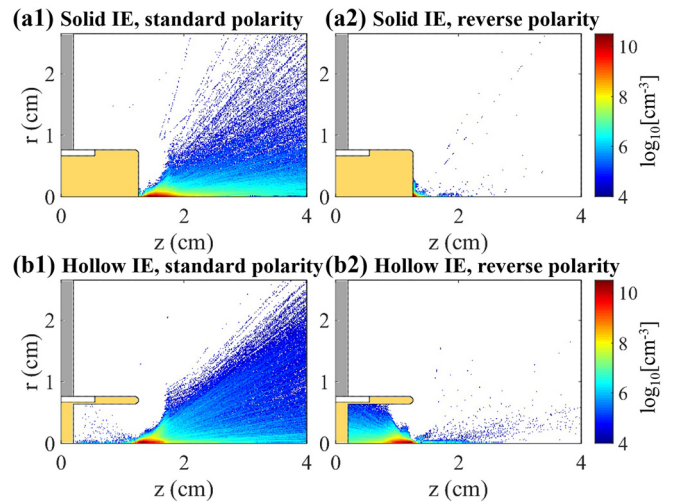


FIG. 4. Number distribution of neutron birth location (on a log scale) in r-z coordinates for (a1) solid IE and standard polarity, (a2) solid IE and reverse polarity, (b1) hollow IE and standard polarity, and (b2) hollow IE and reverse polarity. Each neutron (macro) particle in the simulation was recorded at the position where it was born. Each distribution is taken from one certain run for each case; nevertheless, it is quite representative. The distributions from other identical runs have the same features. We also plotted the electrode positions as a reference.

mechanism. Similar behavior has been observed before on a 3.3 kJ DPF with regular polarity, where only less than 15% of the neutrons were produced within the pinch column, and more than 85% of the neutrons arose from the deuteron beam bombardment of the deuterium gas in the region that was a few cm away from the end of the anode.³⁰ The ion beam is accelerated by a large electric field caused by the $m = 0$ instability. The E field is approximately in the same direction as the current flow; therefore, it points away from the anode in the standard polarity case and towards the cathode in the reverse polarity case. Comparing the solid IE case in Figs. 4(a1) and 4(a2), with reverse polarity, the axially flowing deuteron beam is stopped at the IE surface; hence, the amount of the D target that the beam encounters is tremendously reduced. This is actually the main reason for the order of magnitude decrease in neutron yield. Meanwhile, if a hollow IE is operated under reverse polarity, shown in Fig. 4(b2), the deuteron beam traveling towards the negative IE can still interact with the dense plasma and gas targets inside the hollow. As a result, the neutron yield is much higher than it is in Fig. 4(a2).

With a hollow anode, the pinch location is approximately aligned with the tip of the inner electrode in the axial position z . This can be seen in Fig. 2(b). Assume that the tip of IE is located at $z = z_0$. We found that the neutron spatial distributions in Figs. 4(b1) and 4(b2) are roughly mirrored across this z_0 location. Figure 3(d) shows the neutron creation number distribution as a function of z . The dashed black line indicates the tip of the IE, z_0 . The standard (purple) and reverse (orange) dashed lines both start at $z = z_0$ but extend towards different directions. The reverse case line is somewhat lower than the standard case line due to the limited space in the radial direction inside the hollow. During the run-in, the leading edge of the current sheath is approximately located at $z = z_0$, as shown in Fig. 2(b). Therefore, during the pinch, the $m = 0$ instability is easily seeded at this z_0 position on axis. The amount of plasma target on either side of the instability does not vary a lot from run-to-run. DPF with a solid IE, on the other hand, has the sheath leading edge roughly along the wall of its IE. Compared to the hollow IE case, the left half of the sheath is cut off by the IE wall. The instability could happen at any z location within the pinch region, and the neutron yield is quite sensitive to that, especially for the reverse polarity case. The standard (blue) and reverse (red) curves in Fig. 3(d) illustrate the resulting neutron birth positions. The pinch location is somewhere beyond z_0 but close to it, and the two curves look entirely different. This explains the reason why the hollow anode has much better repeatability regardless of its polarity, as is displayed in Table I. By contrast, a solid IE with reverse polarity has the worst variability of 60.9%, much larger than any other cases. In this particular case, the target quality largely depends on the size of the gap between the location of $m = 0$ instability and z_0 , as well as the amount of deuterons that can pile up within the gap. This adds an additional layer of uncertainty and it explains why the run-to-run variation is large.

The volume of the gas target in Fig. 4(b2) for reverse polarity equals the volume inside the cathode hollow, which is still less than the target volume in standard polarity (b1). To quantify this geometric effect, we consider two regions L and R shown in Fig. 5(b1). They are of the same size and contain the same amount of deuterium gas to start with. The pinch happens just in between them at approximately $z = z_0$. For better comparison, we also define the same region R for solid IE, as shown in 5(a1). Region L does not exist for this geometry. A

statistic according to this region division can be found in Table I. During the pinch, the high energy D beam tends to move towards either L or R depending on the polarity of the device. The region where the majority of D ions enter will generate more neutrons, which we call the “majority region,” while the other region is called the “minority region.” For standard polarity, region R in Figs. 5(b1) and 5(b2) is the majority region and region L is the minority region. For reverse polarity, the opposite is true. Table I shows the neutron yield Y_n in different regions. With a hollow IE, Y_n in the majority region is almost two orders of magnitude higher than the yield in the minority region. Meanwhile, inside the majority region, reverse polarity is only 20% lower in neutron yield compared to standard polarity. With a solid IE, neutrons from reverse polarity can only be produced in the minority region, while the majority of the ion beam impacts into the solid IE. As a result, the overall neutron yield is an order of magnitude lower than standard polarity. The large difference between a solid and a hollow IE indicates that the geometry effect is the main cause of the low yield in reverse polarity.

In the sections that follow, we will examine the quality of beam and target separately.

B. Deuteron beam

In our simulations, the spectrum of the D ion beam was measured by recording ions passing through planes at $z = 4$ cm, $z = 0.2$ cm, and $r = 0.64$ cm. These ions were then divided into 2 groups, $z > z_0$ and $z \leq z_0$, according to their position z , where z_0 is the z position of the tip of the IE at 1.26 cm. The results are shown in Fig. 5(a2) (for solid IE) and (b2) (for hollow IE). The y axis is on a log scale.

Similar to the way we treat neutrons, we divide beam ions into majority and minority groups according to the directions they are traveling, and check their spectra, $f_D(E)$, respectively. The blue curves represent standard polarity and the red curves represent reverse polarity, while darker colors indicate the majority direction and lighter curves indicate the minority direction. The deuteron beam in the minority direction is lower in energy and much less in number compared to the ones in the majority direction; therefore, we can focus on the majority curves. In the case of a hollow IE in Fig. 5(b2), the dark red curve for reverse actually contains more deuterons than the dark blue curve for standard polarity. However, standard polarity produces more ions in the high energy regime above 0.4 MeV. To get a better estimate of the beam quality, we have also plotted $f_D(E) \cdot \sigma(E)$ as a function of E in (b3), where $\sigma(E)$ is the D-D neutron cross-section. The background target density in DPF using deuterium gas is far below solid density even inside the pinch, so the thin target approximation can be applied, which neglects the D ion slowing-down inside the target. As we can see, the minority deuterons [light blue and light red curves in (b3)] make negligible contribution to the total neutron yield. With a hollow IE, the dark blue curve for standard polarity peaks at about 0.4 MeV. The contribution shifts towards the low energy end for reverse polarity, with the dark red curve peaking at 0.06 MeV. The integrated cross section is calculated in Table I. The value from reverse polarity is higher than that from standard, by about 18%. This means that with a thin target, beam quality from reverse polarity is at least compatible to standard.

In order to evaluate the most optimistic scenario for beam-target neutron generation, we have also calculated the number of neutrons that could be produced with our D ion beam traveling into an

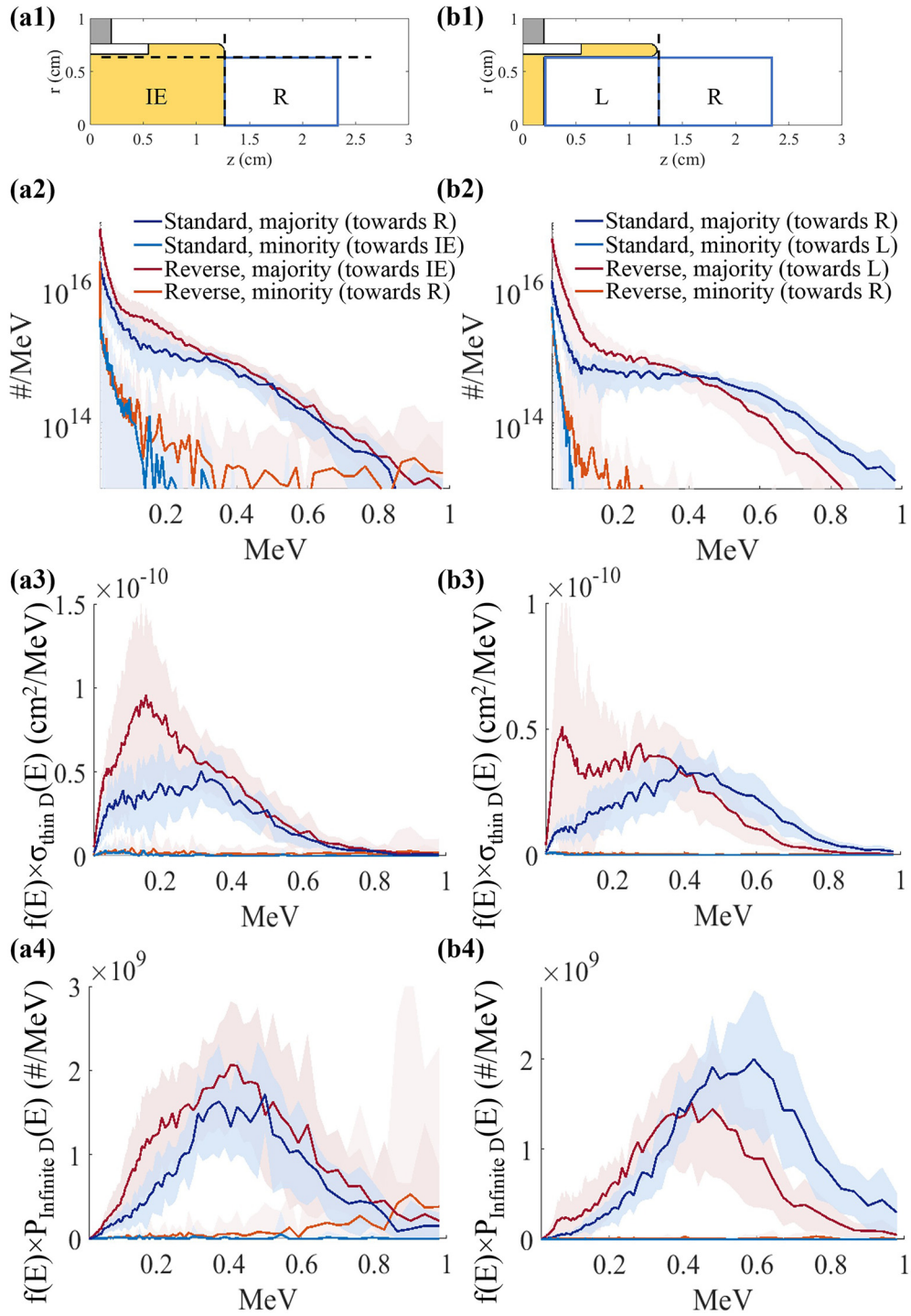


FIG. 5. Deuteron Energy spectra in different directions and the corresponding integrated cross sections. (a) is for solid IE and (b) is for hollow IE. (a1) and (b1) show the way to divide the simulation grid into regions L and R with the same volume for neutron statistics. (a2) and (b2) show the deuteron energy spectra averaged over 10 identical runs. The 4 curves, respectively, represent the majority and minority parts of D beam with standard and reverse polarities, as has been indicated in the legend. Here, majority means the part of D beam heading towards Region R for standard polarity and Region L (or IE) for reverse polarity, and the rest of beam is defined as the minority. Shaded areas behind the curves indicate the standard deviation between runs. (a3) and (b3) show the product of the D spectrum $f_D(E)$ and thin target D-D cross section $\sigma_{\text{thin D}}$ as a function of energy. (a4) and (b4) are the product of $f_D(E)$ and the neutron generation probability with infinitely thick deuterium $P_{\text{Infinte D}}$. They are both straightforward measurements of beam quality.

infinitely thick, cold, liquid deuterium. Figure 5(b4) shows $f_D(E) \cdot P_{Inf,D}(E)$, where $P_{Inf,D}(E)$ is the thick-target neutron generation probability

$$P_{Inf,D}(E) = \int_0^{\infty} \sigma(E(x)) \cdot n_D(x) dx, \quad (1)$$

where x is the deuteron trajectory, n_D is the background ion density, and E is the deuteron energy. Here, E changes as a function of x as the deuteron ion slows down during its transport. The peaks of both dark blue and dark red curves shift to higher energies. The integrated probability, which is also the theoretical maximum yield one could possibly achieve from the given spectrum, is 8.85×10^8 for standard polarity and 6.25×10^8 for reverse polarity. Note that both numbers are about one to two orders of magnitude higher than our current yield.

Now consider the case of solid IE. In the majority direction, the reverse polarity clearly generates a competitive spectrum [Figs. 5(a2)–5(a4)]. Unfortunately, these deuterons all travel into the solid IE, without getting a chance to interact with any decent target. The minority deuterons are actually the ones that generate neutrons in this reverse polarity case, which leads to a poor yield.

Comparing the achieved yield from simulations and the ~ 100 times higher calculated yield from a thick-target, we note that the D beam has not been fully utilized. One way to address this problem is to add an additional deuterated target with solid density as a catcher. For standard polarity, the catcher has to be placed quite a distance away from IE in order to be outside the sheath region. However, the deuteron beam has a large divergence angle which can be seen in Figs. 4(a1) and 4(b1), so it is hard to capture all deuterons. At the same time, another problem in reality is that the metal from the inner electrode tends to sputter and coat the front surface of this catcher target. After several shots, the coating layer can be thick enough to stop the D beam from reaching the deuterated material. These problems may be avoided using a hollow IE with reverse polarity. We can coat the inside of hollow with a thick layer of deuterated material, which may erode over time but likely would not get coated in the anode material. The majority of the D beam will travel into the hollow and get captured entirely. To get an estimate, we calculated the neutron yield assuming we can use a thick layer of cold CD₂. The result is 2.69×10^8 , also shown in Table I. Reverse polarity therefore has potential to significantly increase the neutron yield.

C. Electric field

The D beam is accelerated by a strong electric field due to $m=0$ instability. E field strength during the pinch time directly determines the beam quality. According to Fig. 3(b), the neutrons are produced from 180 ns to 200 ns. We took an average of the electric field over this time window and the results are shown in Fig. 6.

For a hollow IE, Figs. 6(b1) and 6(b2) show the average Ez field for standard and reverse polarities. The fields have similar magnitude of about 4000 kV/cm, but are with opposite signs. This explains why the major deuteron beams are accelerated in opposite directions. The simulated E fields are also consistent with the deuteron energy spectra which show a maximum deuteron energy of about 100 s of keV to MeV. In fact, this E field strength also agrees with other experimental ion spectra on various DPPFs with regular polarity.^{16,33–36} To better understand the formation of this strong E field, we have also added a

contour plot of the average deuteron density (black dashed lines). Three contour lines stand for densities of $10^{16.5} \text{ cm}^{-3}$, 10^{17} cm^{-3} , and $10^{17.5} \text{ cm}^{-3}$, which are labeled in the plots. The initial D density is close to $10^{16.5} \text{ cm}^{-3}$. A more detailed view of the D density distribution is displayed in Fig. 7. From the plots, we can tell where the sheath breaks due to the $m=0$ instability. The E field arises from the reduced conductivity in the gap and extends further within the low density region. Its spatial distribution forms a thin-line shape. The current flows from left to right inside the sheath for standard polarity, so the Ez field also points to the right, and the opposite is true for reverse polarity. The E field only starts to grow after the current flow inside the sheath encounters a sudden break-up. As a consequence, the shape of the E field distribution tends to incline towards the part of sheath that has passed the instability, that is to say, incline to the right for standard and left for reverse polarity. Figures 6(d1) and 6(d2) show the magnitude and direction of the total E field (in the xz plane since the simulation is 2D). The E field direction is almost perpendicular to its “line-shaped” spatial distribution, pointing along the steep change in ion density. Each graph in Fig. 6 only displays one representative run for each particular case. We did not average over 10 simulations as we did for other figures. However, for the hollow IE, all runs look quite similar and share common features that we discussed above.

For a solid IE, on the other hand, run-to-run variations are much larger. The $m=0$ instability grows randomly in a wider region, causing various E field distributions. Figures 6(a1), 6(c1), 6(a2), and 6(c2) only represent one run-in either polarity. Other runs may look different. For standard polarity, the spatial shape of the E field also inclines towards the portion of the sheath that is after its own break-up, while for reverse polarity, E field distribution inclines towards the inner electrode and tends to follow the shape of the IE surface and therefore looks much more straight. The field strengths are again compatible for both polarities, which is consistent with the fact that the ion beams they produce have similar qualities.

D. Deuteron plasma “target”

We have shown that standard and reverse polarities can generate an E field with similar strength in the pinch region and then accelerate a beam of high energy deuterons with compatible quality for neutron production. Next, we evaluate the density of the background deuterons that the high energy beam can interact with, which we call the plasma target. In Fig. 7, we show the deuteron density distribution averaged over the pinch time 180 ns–200 ns.

Checking the results for hollow IE in Figs. 7(b1) and 7(b2), once again we notice the low density gap inside the pinch due to the $m=0$ instability, and besides it is the background target. The plasma target density is on the order of 10^{18} cm^{-3} within the pinch region. According to Sec. III C, for standard polarity, only the portion of target to the right of the instability gap affects yield, while for reverse polarity, only the left portion matters. Comparing Figs. 7(b1) and 7(b2) to the neutron distribution in Figs. 4(b1) and 4(b2), it seems that the area with the highest ion density also produces the largest amount of neutrons. Inside the pinch region, the plasma target from standard polarity looks slightly better than that from reverse polarity. This is reasonable since according to Table I, the beam quality (measured by the integrated thin target cross section $\int f_D(E) \cdot \sigma_{thinD}(E) dE$) from reverse polarity is slight better than standard, while the neutron yield in Region L for standard is higher than that in Region R for reverse.

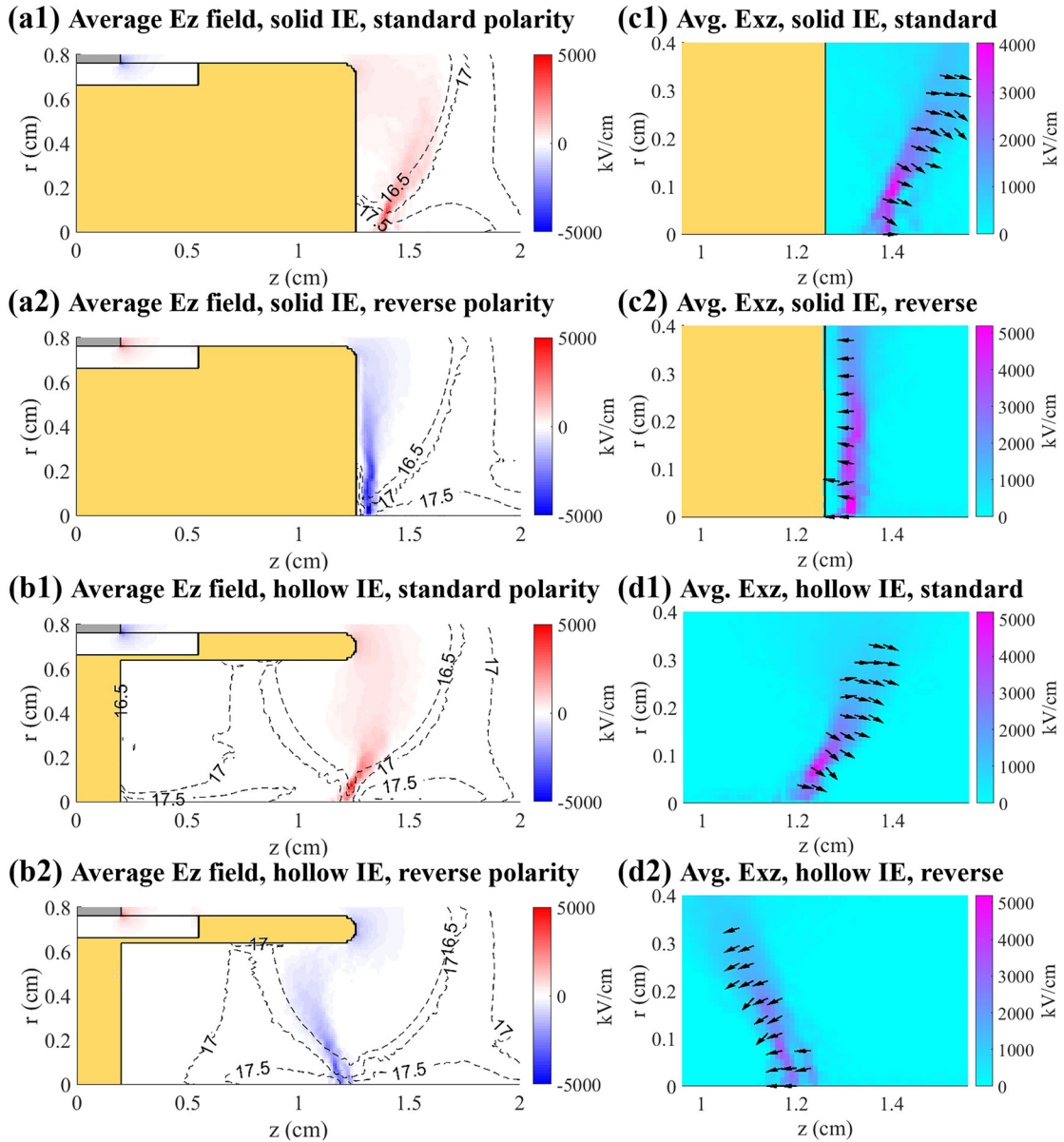


FIG. 6. E_z and total \mathbf{E} field averaged over the pinch time. Here, all plots are averaged over a 20 ns time window (180 ns–200 ns), which is the duration of the neutron pulse. Note that we did not further average over 10 runs, so each plot only represents one certain run. For a hollow IE, different runs share similar features so (b1), (b2), (d1), and (d2) can represent the general case. For a solid IE, on the other hand, the run-to-run variation is quite large, so (a1), (a2), (c1), and (c2) can change in another run. The E_z component is plotted in (a1), (a2), (b1), and (b2). A contour of the averaged deuterium density is also plotted as the dashed black lines. They represent the densities of $10^{16.5} \text{ cm}^{-3}$, 10^{17} cm^{-3} , and $10^{17.5} \text{ cm}^{-3}$ and are labeled as “16.5,” “17,” and “17.5,” respectively. The \mathbf{E} field (in the xz plane) is plotted in (c1), (c2), (d1), and (d2) with its magnitude indicated by the color bar and its direction indicated by the arrows.

Standard polarity also has an additional target volume outside Region R with the initial deuterium gas density. Despite the low density, this region is responsible for about 24% of the total neutron yield. The overall neutron yield from standard is 38% higher than reverse, and this additional target contributes greatly to the additional yield.

For solid IE, the standard polarity in Fig. 7(a1) has a high-density plasma target that is similar to that in (b1). However, the reverse

polarity hardly has any target to the left of the instability. As a consequence, the neutron yield is an order of magnitude lower than standard polarity.

IV. SUMMARY

To conclude, we have performed PIC simulations for a small DPF device with both standard and reverse polarities. This is the first

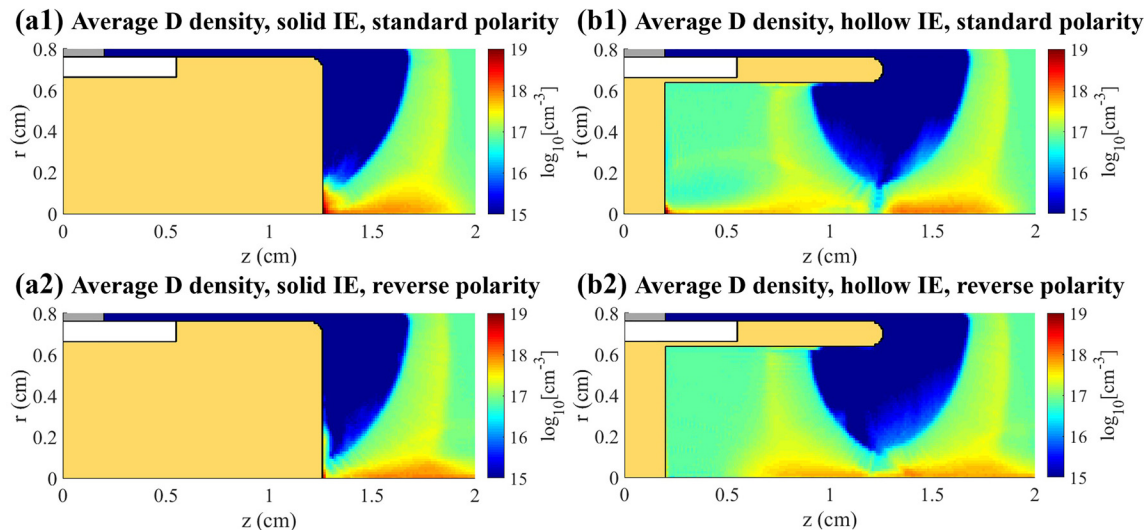


FIG. 7. Deuteron density n_D distribution averaged over the pinch time (180 ns–200 ns). Each plot represents a certain run for a particular case: solid IE with standard polarity (a1), solid IE with reverse polarity (a2), hollow IE with standard polarity (b1), and hollow IE with reverse polarity (b2). We have performed 10 runs for each case and the average n_D all look similar to the plot we show here.

time that polarity riddle has been carefully studied with simulations. We have tried two different inner electrode (IE) geometries, one is a solid cylinder and the other has a large hollow in the center. With a solid IE, reverse polarity generates about ten times fewer neutrons than standard polarity, which is consistent with previous experimental results.⁵ To understand this, we have compared the D ion beam spectra and found that their qualities are about the same for both polarities. However, they are traveling in different directions. The beam from reverse polarity was lost in the solid IE, preventing it from producing neutrons. With a hollow IE, this detrimental effect can be largely minimized, so that the resulting neutron yields from both polarities are comparable. We further investigated the high-density plasma target inside pinch with a hollow IE and found that target quality for standard polarity is only slightly better than that for reverse polarity. Contrary to what people have believed for over thirty years, the “notorious” reverse polarity actually produces comparable beam and plasma target to conventional polarity.

While adding an external catcher target to boost the neutron yield is not trivial for standard polarity, reverse polarity with a hollow IE has the advantage of easily collecting high energy ion beams inside its hollow without sputter onto target. This means that we can potentially coat the inner electrode with the deuterated material which serves as a dense catcher. This method has the potential to significantly enhance the neutron yield from reverse polarity to be even higher than standard. We will probe this method for increasing the yield in more detail in future studies.

ACKNOWLEDGMENTS

We would like to acknowledge Christopher Cooper, Justin Angus, Kurt Tummel, Matthew McMahon, Alexei Pankin, Alexander Povilus, and everyone in the DPF group at LLNL for useful discussions and comments. This work was performed under the auspices of the U.S. Department of Energy by Lawrence Livermore National Laboratory

under Contract No. DE-AC52-07NA27344 and supported by the Laboratory Directed Research and Development Program (15-ERD-034) at LLNL. Computing support for this work came from the LLNL Institutional Computing Grand Challenge program.

REFERENCES

- ¹M. Krishnan, *IEEE Trans. Plasma Sci.* **40**, 3189 (2012).
- ²J. R. Smith, C. M. Luo, M. J. Rhee, and R. F. Schneider, *Phys. Fluids* **28**, 2305 (1985).
- ³Y. Kato and S. H. Be, *Appl. Phys. Lett.* **46**, 686 (1986).
- ⁴J. M. Bayley, G. Decker, W. Kies, M. Malzig, F. Muller, P. Rowekamp, J. Westheide, and Y. V. Sidelnikov, *J. Appl. Phys.* **69**, 613 (1991).
- ⁵G. Decker, W. Kies, and G. Pross, *Phys. Lett. A* **89**, 393 (1982).
- ⁶M. Mathuthu, T. G. Zengeni, and A. V. Gholap, *Rev. Sci. Instrum.* **68**, 1429 (1997).
- ⁷M. Mathuthu, T. G. Zengeni, and A. V. Gholap, *IEEE Trans. Plasma Sci.* **26**, 14 (1998).
- ⁸E. L. Ruden, *Phys. Plasmas* **11**, 713 (2004).
- ⁹J. W. Mather, *Phys. Fluids* **8**, 366 (1965).
- ¹⁰T. Oppenlander, G. Pross, G. Decker, and M. Trunk, *Plasma Phys.* **19**, 1075 (1977).
- ¹¹L. Soto, A. Tarifeno-Saldivia, C. Pavez, G. Avaria, J. Moreno, N. Cabrini, and M. Zambra, in *39th EPS Conference 16th International Congress on Plasma Physics* (2012).
- ¹²F. N. Beg, M. Zakaullah, M. Nisar, and G. Murtaza, *Mod. Phys. Lett. B* **6**, 593 (1992).
- ¹³F. N. Beg, M. Zakaullah, and G. Murtaza, *Phys. Scr.* **46**, 152 (1992).
- ¹⁴F. N. Beg, M. Shabbir, M. Zakaullah, and G. Murtaza, *Phys. Lett. A* **186**, 335 (1994).
- ¹⁵A. Schmidt, V. Tang, and D. Welch, *Phys. Rev. Lett.* **109**, 205003 (2012).
- ¹⁶A. Schmidt, A. Link, D. Welch, J. Ellsworth, S. Falabella, and V. Tang, *Phys. Rev. E* **89**, 061101 (2014).
- ¹⁷A. Schmidt, A. Link, D. Welch, V. Tang, C. Halvorson, M. May, and E. C. Hagen, *Phys. Plasmas* **21**, 102703 (2014).
- ¹⁸A. Link, C. Halvorson, E. C. Hagen, D. V. Rose, D. R. Welch, and A. Schmidt, *AIP Conf. Proc.* **1639**, 23 (2014).
- ¹⁹D. P. Higginson, A. Link, and A. Schmidt, “A pairwise nuclear fusion algorithm for weighted particle-in-cell plasma simulations,” *J. Comput. Phys.* **388**, 439 (2019).

- ²⁰Chicago is being developed by Voss Scientific with partial support from the Defense Advanced Research Projects Agency under Contract No. W31P4Q-15-C-0055 and the Air Force Office of Scientific Research under Contract No. FA9550-14-C-0034.
- ²¹D. R. Welch, D. V. Rose, M. E. Cuneo, R. B. Campbell, and T. A. Mehlhorn, *Phys. Plasmas* **13**, 063105 (2006).
- ²²A. Friedman, *J. Comput. Phys.* **90**, 292 (1990).
- ²³C. Thoma, D. R. Welch, R. E. Clark, D. V. Rose, and I. E. Golovkin, *Phys. Plasmas* **24**, 062707 (2017).
- ²⁴K. Nanbu, *Phys. Rev. E* **55**, 4642 (1997).
- ²⁵K. Nanbu and S. Yonemura, *J. Comput. Phys.* **145**, 639 (1998).
- ²⁶D. R. Welch, D. V. Rose, C. Thoma, R. E. Clark, C. B. Mostrom, W. A. Stygar, and R. J. Leeper, *Phys. Plasmas* **17**, 072702 (2010).
- ²⁷D. R. Welch, D. V. Rose, C. Thoma, R. E. Clark, C. B. Mostrom, W. A. Stygar, and R. J. Leeper, *Phys. Plasmas* **18**, 056303 (2011).
- ²⁸D. Klir, J. Kravarik, P. Kubes, K. Rezek, S. S. Ananey, Y. L. Bakshaev, P. I. Blinov, A. S. Chernenko, E. D. Kazakov, V. D. Korolev, G. I. Ustroeov, L. Juha, J. Krasa, and A. Velyhan, *IEEE Trans. Plasma Sci.* **37**, 425 (2009).
- ²⁹B. Appelbe and J. Chittenden, *Phys. Plasmas* **22**, 102703 (2015).
- ³⁰S. Moo, C. Chakrabarty, and S. Lee, *IEEE Trans. Plasma Sci.* **19**, 515 (1991).
- ³¹L. Soto, P. Silva, J. Moreno, M. Zambra, W. Kies, R. E. Mayer, A. Clause, L. Altamirano, C. Pavez, and L. Huerta, *J. Phys. D: Appl. Phys.* **41**, 205215 (2008).
- ³²M. Milanese, R. Moroso, and J. Pouzo, *Eur. Phys. J. D* **27**, 77 (2003).
- ³³H. Bhuyan, H. Chuaqui, M. Favre, I. Mitchell, and E. Wyndham, *J. Phys. D* **38**, 1164 (2005).
- ³⁴W. H. Bostick, H. Kilic, V. Nardi, and C. W. Powell, *Nucl. Fusion* **33**, 835 (1993).
- ³⁵M. Zakaullah, I. Akhtar, A. Waheed, K. Alangir, A. Z. Shah, and G. Murtaza, *Plasma Sources Sci. Technol.* **7**, 206 (1998).
- ³⁶S. V. Springham, S. Lee, and M. S. Rafique, *Plasma Phys. Controlled Fusion* **42**, 1023 (2000).